

KITECH-Hand: A Highly Dexterous and Modularized Robotic Hand

Dong-Hyuk Lee, Jae-Han Park, *Member, IEEE*, Sung-Woo Park, Moon-Hong Baeg,
and Ji-Hun Bae, *Member, IEEE*

Abstract—This paper presents an anthropomorphic robotic hand named “KITECH-Hand,” along with its kinematic analysis and detailed mechanical features. From a kinematic perspective, the authors particularly focus on the structure of the metacarpophalangeal (MCP) joints of the fingers. The KITECH-Hand adopts a new “roll-pitch”-type MCP structure to replace conventional “yaw–pitch” structures. The proposed structure provides benefits such as enhanced kinematic performance and ease of the mechanical design. Through the kinematic analysis, it is shown that the KITECH-Hand shows remarkably high dexterity, well surpassing that of existing robotic hands with conventional MCP joints. The unique MCP structure also helps modularize the robot at the joint level, which simplifies its mechanical structure and enables the production cost to be reduced. The performance of the KITECH-Hand, including its dexterity feature, was experimentally verified through a series of experiments, which included object in-hand manipulation and a Cutkosky taxonomy test.

Index Terms—Dexterous manipulation, robot hand, thumb opposability.

I. INTRODUCTION

IN ROBOTIC object manipulation research, even seemingly simple tasks may require an extremely high manipulation capability. Such tasks can typically be found in factory assembly lines, e.g., mating parts and packaging boxes. A simple solution for these tasks is to prepare specialized tools designed for a single task and change the tools depending on the given situation. Although this is, at present, the dominant approach for factory

Manuscript received February 19, 2016; revised August 2, 2016; accepted October 27, 2016. Date of publication December 1, 2016; date of current version April 14, 2017. Recommended by Technical Editor Y. Tian. This paper was presented in part at IEEE/RSJ International Conference on Intelligent Robots and Systems, Vilamoura, Algarve, Portugal, Oct. 7–12, 2012. This research was supported by Basic Science Research Program through the National Research Foundation of Korea (NRF) funded by the Ministry of Education(2016R1A6A3A04012911).

D.-H. Lee, J.-H. Park, M.-H. Baeg, and J.-H. Bae are with the Robot Cognition and Control Laboratory, Robot R&D Group, Korea Institute of Industrial Technology, Ansan 15588, South Korea (e-mail: donghyuk@kitech.re.kr; hans1024@kitech.re.kr; mhbaeg@kitech.re.kr; joseph@kitech.re.kr).

S.-W. Park is with MECHA TNS (e-mail: notablepark@gmail.com).

This paper has supplementary downloadable material available at <http://ieeexplore.ieee.org>.

Color versions of one or more of the figures in this paper are available online at <http://ieeexplore.ieee.org>.

Digital Object Identifier 10.1109/TMECH.2016.2634602

automation, it increases cost and time. Furthermore, some tasks are hard to automate without human-level dexterity, e.g., tying cables. Anthropomorphic robotic hands have the potential to enable human-level versatility, which allows a wider range of tasks to be carried out in various situations.

So far, robot hands have been implemented by closely mimicking the mechanical structure of the human hand. Each finger of the human hand contains three joints: the metacarpophalangeal (MCP), proximal interphalangeal (PIP), and distal interphalangeal (DIP) joints (in this paper, the word “fingers” does not include the thumb). The PIP and DIP are single-degree-of-freedom (DOF) joints allowing flexion and extension. The MCP is a two-DOF joint enabling flexion/extension and abduction/adduction of the finger. The PIP and DIP joints are simple and relatively easy to realize. In contrast, two joints in the MCP whose axes intersect cause complexity in the robot hand design and hinder modularization at the joint (phalange) level. This paper specifically considered the mechanical implementation of MCP joints in robot hands and attempted to find an alternative way to cover its functionality.

Most of the previous robot hands utilized two-DOF “yaw–pitch”-type MCP joints, which provided motions equivalent to those of a human hand. In this type of joint, the “yaw” and “pitch” movements enable abduction/adduction and flexion/extension, respectively. A “yaw–pitch” joint can be physically implemented in various ways. An MCP design using a differential mechanism with four bevel gears has been widely used in various previous robot hands including the DLR-Hand II [1], the Gifu-Hand series [2], [3], and SKKU-Hand IV [4]. Ryew and Choi proposed an MCP mechanism called a “double active universal joint,” which enlarged the range of motion using two serially connected universal joints [5]. ACT hand introduced by Matsuoka *et al.* showed an MCP mechanism driven by anatomically correctly aligned tendon mechanism [6]. CEA-hand introduced a backdrivable MCP design using ball-screw and tendon-driven mechanism [7], [8]. A number of robot hands adopted an MCP design whose two axes do not intersect to ease the mechanism design. These types of design can be seen in UB-hand series [9], [10] and Robonaut 2 hand [11].

It is known that the existence of the MCP joint enables dexterous object manipulation by creating an overlapped area of workspace between fingers [3]. However, it is questionable whether the “yaw–pitch”-type joint is the only possible option for implementing MCP joints covering the human-level functionality.

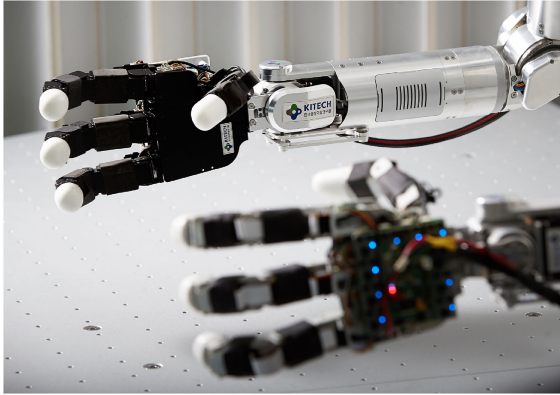


Fig. 1. KITECH-Hands attached on the anthropomorphic robotic arms.

In this research, a robotic hand modularized to the joint level with a unique MCP joint structure is presented. This paper shows that the proposed MCP structure not only enables low-cost production by enabling the modularization, but also increases the dexterity of the robotic hand. A prototype of the KITECH-Hand was previously built focusing on low cost [12]; however, its important characteristics including its kinematic benefits were not addressed. This paper presents an improved version of the robotic hand in terms of the mechanical and electronic design, as shown in Fig. 1, with a detailed explanation of its design and kinematic benefits. Based on the principle of modularization, the KITECH-Hand was designed according to detailed design goals.

Affordability: Compact commercial servo modules are used as the actuator modules of the robotic fingers. Their all-in-one configuration including an electric motor, a speed reducer, and an absolute position sensor helps to build the robotic hand in a mechanically simpler fashion at lower cost.

Backdrivability: The mechanical backdrivability is important for the robot hands, which frequently experience physical contact with environment. The backdrivable joints of the KITECH-Hand allow the contact force control in a feedforward manner without costly F/T sensors.

Embedded circuits: Since the robotic hand consists of many joints (generally more than ten), space for the driving circuitry is another issue when designing the robotic hand. In this research, all the driving circuits are embedded into the robotic hand, and thus, no external space is required.

Lightweight: The robotic hand should be designed as light as possible due to the payload limitation of the manipulators. Most of the existing robotic hands weigh more than 1 kg, which limits the allowable payload for the object manipulation. The KITECH-Hand is designed to weigh less than 1 kg, including embedded electronics.

This paper is organized as follows. In Section II, a proposed kinematic structure of the robotic hand is introduced, and its kinematic performance is analyzed. Section III presents the mechanical and electronic design of the robotic hand in detail. Experimental verification and evaluation results are provided in Section IV. Finally, the paper is concluded in Section V.

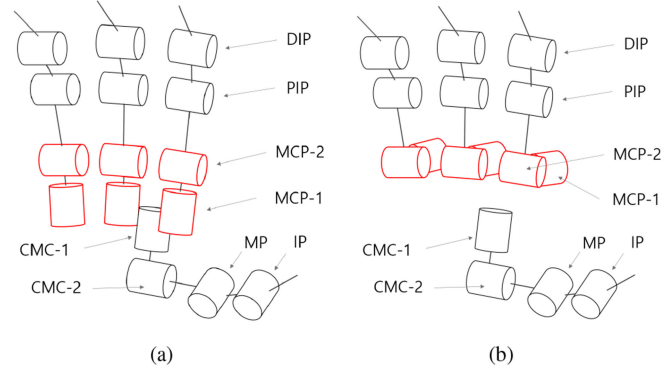


Fig. 2. Kinematic structure of the KITECH-Hand and the C-Hand (The MCP joint of thumb is referred as “MP” to avoid confusion with MCP of fingers). (a) KITECH-Hand. (b) C-Hand.

II. KINEMATIC ANALYSIS

A. Kinematic Model

In this paper, the authors propose a new kinematic structure of a robotic hand (referred as the KITECH-Hand), as shown in Fig. 2(a). The key difference from conventional robotic hands is the “roll–pitch”-type MCP joint of the fingers. As shown in the figure, the first joint in the MCP (MCP-1) enables the rolling motions of the finger, and the second joint (MCP-2) implements flexion and extension of the finger. In this structure, the rolling motion of the finger replaces the abduction and adduction of human fingers.

Although the rolling motion does not exist in the human hand structure, in this research, the authors claim that it can effectively cover most grasping motions of the human hand. More importantly, the proposed structure provides benefits with respect to the kinematic performance and the mechanical design of the robotic hand. This section analyzes the kinematic benefits of the proposed structure.

For proper evaluation of the kinematic performance of the proposed structure, another kinematic structure is introduced by way of comparison, as shown in Fig. 2(b). The only difference from the proposed model shown in Fig. 2(a) is its “yaw–pitch”-type MCP joints. This model represents robotic hands with a conventional MCP structure. In this section, the model is referred as conventional-Hand (C-Hand). The main advantage of the C-Hand is its similarity to the human hand. The first and second joints in the MCP realize abduction/adduction and flexion/extension of the fingers, analogous to the human hand. On the other hand, from a mechanical perspective, this type of joint structure is not easy to implement in a direct-driven manner because of the alignment of the first joint (MCP-1).

The KITECH-hand and the C-hand have the same range of motion and phalange lengths, as listed in Table I. The kinematic parameters of the robot hands were determined based on the typical human hand structure. The next subsection addresses the benefits of the proposed structure in terms of kinematics.

TABLE I
KINEMATIC PARAMETERS OF THE KITECH-HAND AND THE C-HAND

Type	Joint	Range of motion	Phalange length [mm]
Finger	MCP-1	-33–33°	—
	MCP-2	-15–95°	54.0 (MCP-2 to PIP)
	PIP	-15–95°	38.4 (PIP to DIP)
	DIP	-15–95°	36.0 (DIP to fingertip)
Thumb	CMC-1	0–70°	—
	CMC-2	0–75°	53.0 (CMC-2 to MP)
	MP	-15–95°	38.4 (MP to IP)
	IP	-15–95°	59.0 (IP to fingertip)

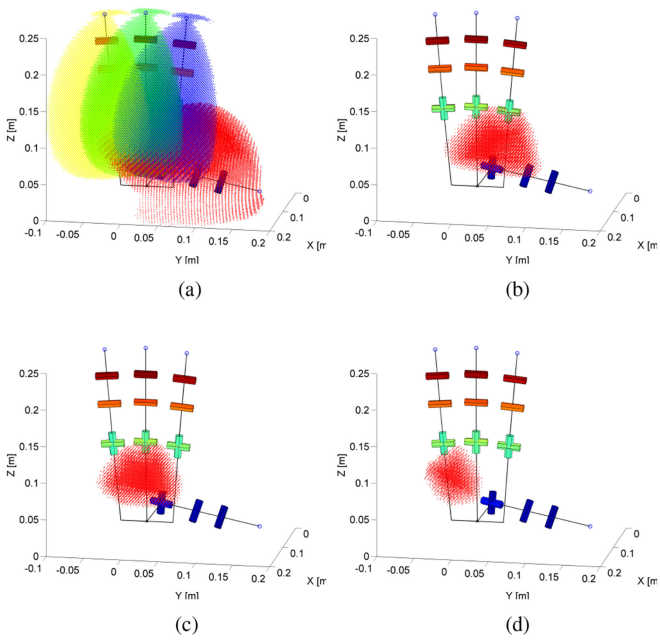


Fig. 3. Workspace of the KITECH-Hand. (a) Total workspace. (b)–(d) Common workspace of the thumb–index, thumb–middle, and thumb–ring fingers, respectively.

B. Workspace and Thumb Opposability

It is known that an opposable thumb is key to the dexterity of human hands [2], [3], [13]. This can be explained more specifically using the concept of the common workspace [3], i.e., an opposable thumb creates an overlapped volume of the workspace between the thumb and fingers, which results in the ability to control the force or the position of a grasped object. Therefore, it is reasonable that the wider the common workspace, the better the dexterous grasping.

Although it is not explicitly stated in the literature, it is obvious that the workspace volume of the fingers contributes to increase the volume of the common workspace. Since the PIP and DIP joints in most of the anthropomorphic robotic hands have a similar range of motion, the MCP joints crucially affect the workspace volume of the finger. The kinematic advantage of the KITECH-Hand derives from this property.

Fig. 3(a) shows the total workspace of each finger and the thumb of the KITECH-Hand. The workspaces were obtained using the Monte–Carlo-based method proposed by Rastegar and

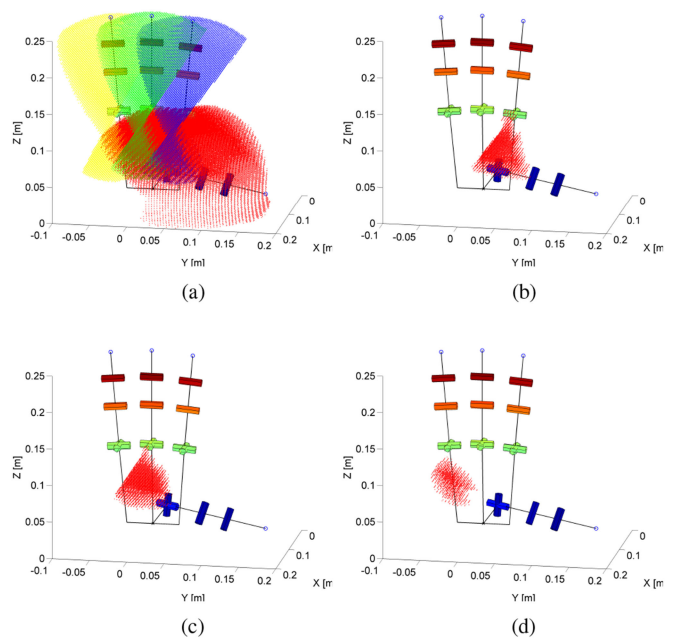


Fig. 4. Workspaces of the C-Hand. (a) Total workspace. (b)–(d) Common workspace of the thumb–index, thumb–middle, and thumb–ring fingers, respectively.

Fardanesh [14]. Note that the kinematic singular point of each finger appears at the top of its workspace. This is caused by the proposed MCP structure. The total volumes of the workspace of the thumb and fingers are 607 and 687 cm³, respectively (the workspace volume is the same for each finger).

Meanwhile, the total workspace of the C-Hand is shown in Fig. 4(a). The figure effectively visualizes the finger’s fan-shape workspace, which is different from that of the proposed model. In this case, the kinematic singular points of the fingers are located in the middle of the workspace, as shown in the figure. This feature causes a difference between the workspace volumes of the two models. In the C-Hand, the total volume of the workspace of the finger is 527 cm³, which is 23.3% smaller than that of the KITECH-Hand.

The difference in the workspace volume creates a difference between the common workspace volumes of the two models. Fig. 3(b)–(d) shows the common workspaces between the thumb and each finger of the proposed model. As shown in the figures, the volume of the common workspace decreases in the order thumb-to-index-finger, thumb-to-middle-finger, and thumb-to-ring-finger. The absolute values of the common workspace volumes are listed in Table II. For comparison, the common workspaces of the C-Hand are obtained as shown in Fig. 4(b)–(d). As listed in Table II, the volumes of the common workspaces are calculated to be 44%, 39%, and 50% smaller than that of the KITECH-Hand for the thumb–index, thumb–middle, and thumb–ring finger combinations, respectively. These differences can be easily understood by considering the locations of the singular points shown in Figs. 3(a) and 4(b).

The common workspace volumes of a number of existing robotic hands are listed in Table II, along with those of the KITECH-Hand and the C-Hand. These volumes were calculated

TABLE II
WORKSPACE INTERSECTION VOLUMES OF THE KITECH-HAND AND THE EXISTING ROBOTIC HANDS

	v_1 [mm ³]	v_2 [mm ³]	v_3 [mm ³]	v_4 [mm ³]
KITECH-Hand	175 803	165 811	81 693	n/a
C-Hand	97 587	101 207	40 665	n/a
Gifu-Hand III	62 500	47 500	49 900	12 900
DLR-Hand	37 941	12 103	6171	838
UB-Hand 4	24 516	32 131	8797	0
SKKU-hand IV	44 020	43 522	6439	n/a

TABLE III
THUMB OPPOSABILITY OF THE KITECH-HAND AND THE EXISTING ROBOTIC HANDS

	n	d [mm]	Thumb Oppo. [$\times 10^{-2}$]
KITECH-Hand	3	150.4	12.413
C-Hand	3	150.4	7.039
Gifu-Hand III	4	156.7	4.49
DLR-Hand	4	148	2.494
UB-Hand 4	3	95	2.400
SKKU-Hand IV	3	215	0.494

from known specifications of the hands (the values of Gifu-Hand III were extracted from [3]). Since the listed values depend on the physical dimension of the finger, they cannot be directly used to compare the dexterity of the robotic hands.

Thumb opposability is a performance index introduced by Mouri *et al.*, designed to evaluate the dexterity of a robotic hand [3] based on the observation that the common workspace volumes between the thumb and the fingers crucially determine the grasping performance of robotic hands. The thumb opposability J is defined as follows:

$$J = \frac{1}{d^3} \sum_{i=1}^n w_i v_i \quad (1)$$

where v_i denotes the intersection volume of the workspace between the thumb and the i th finger ($1 = \text{index}$, $2 = \text{middle}$, ...). d is the effective length of the thumb, and n is the total number of fingers excluding the thumb. w_i is the weighting factor of the i th finger, which defines the importance of this finger for grasping. In this research, the weighting factors of all fingers are defined as 1.0, following the convention established by the inventor of the method.

The performance index can be used to determine the optimal kinematic configuration of the thumb, as was done for Gifu-Hand III and the revised version of DLR/HIT II hand [13]. In this research, the thumb opposability is used to compare the difference in kinematic capability caused by the “roll–pitch”-type MCP structure.

The thumb opposability values of the KITECH-Hand and the C-Hand were calculated using the definition above; the results are listed in Table III, along with those for a number of existing robotic hands. The values for the workspace intersection volumes v_i in Table II were used to calculate the thumb opposability. As expected, the KITECH-Hand has a dramatically

higher value of the thumb opposability than the existing robotic hands. This results can be explained using the location of singular point in the finger’s workspace. Since the finger’s singular point of the KITECH-Hand locates on the top of the workspace, it could provide the larger common volume with the thumb. Of course, we can see that this difference is caused by the proposed MCP structure.

An interesting result is that the thumb opposability of the C-Hand is also higher than that of the existing robotic hands. It is thought that the result is caused by the kinematic structure of the thumb shown in Fig. 2(a). In fact, the kinematic structure of the thumb in the KITECH-Hand is somewhat different from that of previous thumb designs. Similar to the MCP joints of the fingers, the second joint of the CMC (CMC-2) creates the roll motion of the thumb. The purpose of this mechanism is the same as for conventional CMC joints; however, the roll joint makes the thumb’s opposable pose easier. Although an analytical comparison with the conventional thumb structure is not easy due to the variety of previous thumb designs, the dexterous capability of the thumb of the KITECH-Hand is demonstrated in Section III-B using Kapandji tests.

C. Manipulability

Although the thumb opposability is a useful index to quantify the overall dexterity of robot hands, it does not provide information regarding how dexterous the robot hand is at a specific pose or task. In the field of robotics, the term “dexterity” is defined as an ability to move and apply forces in arbitrary direction with equal ease [15]. This definition implies that the dexterity depends on the pose or specific task. In this subsection, we analyze the dexterity of the proposed robot hand using a concept of kinematic manipulability and find a task the KITECH-Hand can perform better than the conventional robot hands.

The manipulability ellipsoid is a well-known tool to evaluate the dexterity of a robot manipulator [16]. Each length of the principal axis in the ellipsoid indicates the relative degree of “ease” of motion along the axis. Fig. 5(a) and (b) shows the manipulability ellipsoids with respect to index finger of the KITECH-Hand and the C-Hand, respectively. In both cases, joint angles of the index finger were [0111] in radians. Note the difference of the manipulability in the Y -axis. The difference is generated due to the location of singular point discussed in the previous subsection. Since the singular point of the C-Hand locates inside of the common workspace (see Fig. 4), Y -directional motion of the fingertip is easily restricted during object grasping. This property can be confirmed more specifically using the spatial distribution of the manipulability. The manipulability measure (MM), which corresponds to the volume of the manipulability ellipsoid, is a useful index to express the degree of dexterity in the 3-D space and is defined as follows:

$$w = \sqrt{\det(\mathbf{J}(\mathbf{q})\mathbf{J}(\mathbf{q})^\top)} \quad (2)$$

where $\mathbf{J}(\mathbf{q})$ denotes a Jacobian matrix at the posture \mathbf{q} of the finger (or thumb). Since the Jacobian matrix is the function of joint posture, for a redundant manipulator, there exists an infinite number of MMs at an arbitrary point in the space. The fingers

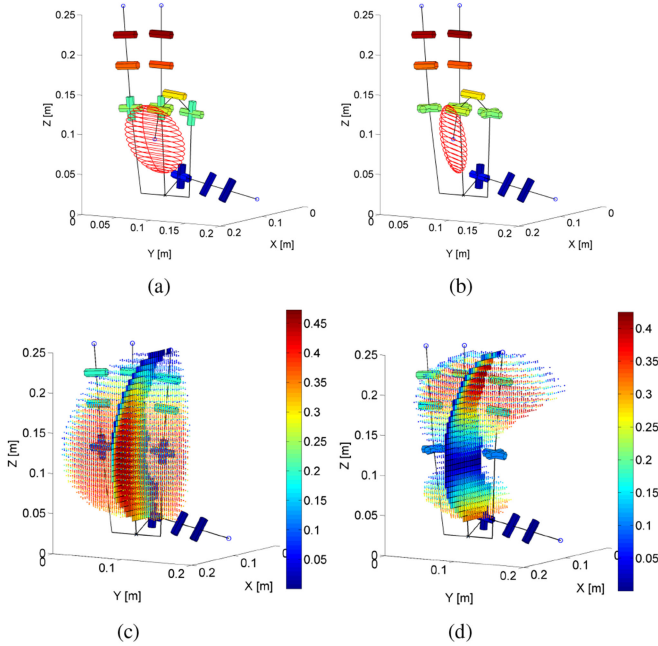


Fig. 5. (a) and (b) Manipulability ellipse of the index finger of the KITECH-Hand (left) and the C-Hand (right), respectively. (c) and (d) Distribution of the mean MM of the KITECH-Hand (left) and the C-Hand (right), respectively.

and thumb in the KITECH-hand can be seen as the redundant manipulator in the 3-D task space. Therefore, it is not easy to visualize distribution of MM in the 3-D space. To effectively visualize the manipulability, we use distribution of mean MM, which is obtained as follows.

- 1) Randomly sample q and consequent MM values in sufficient number.
- 2) Divide the workspace into a grid.
- 3) Calculate mean MM in each grid cell by averaging the samples in the grid cell.

By using a sample size of 540 000 and a $30 \times 30 \times 30$ grid, the distribution of mean MM of each robot hand was obtained. Fig. 5(c) and (d) depicts the distribution of mean MM of the index finger and its cross-sectional view in the xz plane in the KITECH-Hand and the C-Hand, respectively. The two figures show a distinct difference. As shown in Fig. 5(a), the region with high manipulability appears at the central part of the workspace. In contrast, the high-manipulability regions for the C-Hand appear near the upper and lower ends of the workspace, as shown in Fig. 5(d). An important feature expected from this characteristic is the object in-hand manipulation performance of the robot hand. During typical precision grasping tasks, the position of fingertip generally locates in the middle of the finger's workspace, which corresponds to the high-manipulability region of the KITECH-Hand. In the case of the C-Hand, the fingertip locates in the low-manipulability region of the workspace, which results in lower dexterity (note that fingertip's lateral motion is almost restricted during the precision grasping in the case of the human hand). This advantage will be experimentally demonstrated in Section IV-B.

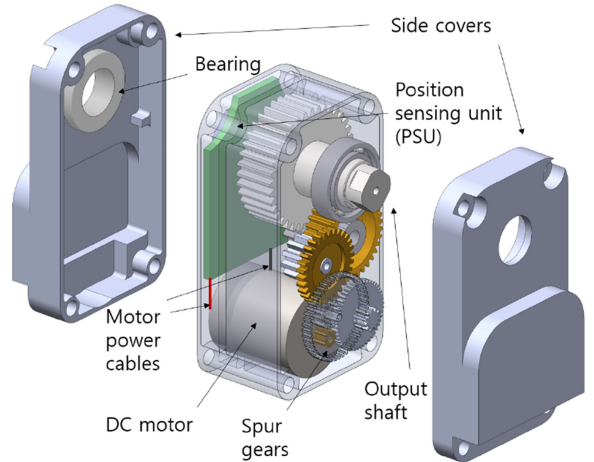


Fig. 6. Internal structure of the actuator module.

III. DESIGN

This section explains the detailed mechanical and electronic design of the robotic hand with an introduction of its low-level control scheme.

A. Modularized Design

As aforementioned, the proposed “roll–pitch”-type MCP structure eliminates the necessity of mechanically complicated 2-DOF universal-joint-like mechanisms. This feature enables modularizing the robotic hand at the joint level by connecting identical joint modules in series. To exploit this advantage, commercial compact servo modules (RS301CR-H3b, HPI, Japan) were used as basic building blocks of the robotic hand. The servo module is chosen mainly for its high power density in a small size. Since the commercial servo modules contain parts that were not necessary for this research, their original configuration was modified with respect to the mechanical housing and the electronics. To avoid confusion, the modified servo modules are called “actuator modules” hereafter. The default side cover of the servo module was removed and replaced by newly designed ones that construct the linkage of the finger. The original electronics of the servo modules were removed and replaced with newly designed current controllers (installed on the palm) and absolute position-sensing units (PSUs) (installed in the actuator module).

Fig. 6 shows the inside configuration of the actuator module. The DC motor generates a maximum driving torque of 0.71 N·m at the output shaft, after passing a speed reduction mechanism using spur gears. Despite the relatively high transmission ratio at the speed reduction mechanism (1:369), the actuator module is backdrivable, which helps with the torque control of the actuator module based on current servoing. The backdrivability can be confirmed in the supplementary movie of this paper. The newly designed PSU, which consists of a potentiometer and an analog-to-digital converter, measures the absolute position of the joint in a 16-bit resolution. The PSU also provides power to the DC motor. The low-level control and electrical details of the

TABLE IV
SPECIFICATIONS OF THE ACTUATOR MODULE

Quantity	Value
Dimension	35.8 mm × 19.5 mm × 25 mm
Reduction ratio	1:369
No load speed	545°/s
Max. torque	0.71 N · m
Weight	40 g
Unit cost (before modification)	\$ 100

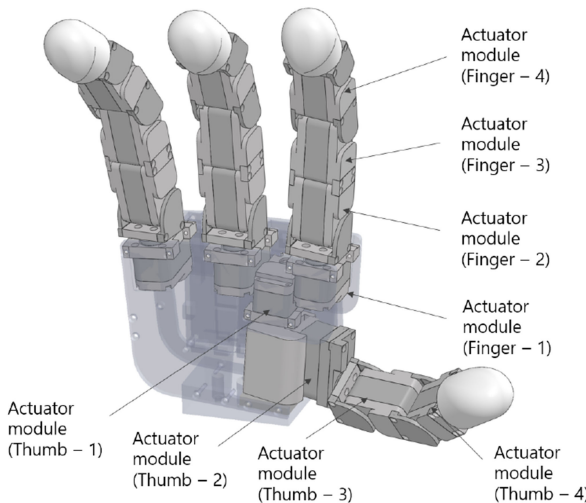


Fig. 7. CAD design of the finger and thumb.

actuator module are addressed in Section III-B. Table IV lists the mechanical and electrical specifications of the actuator module.

The robotic hand was constructed with a thumb and three identical fingers. Fig. 7(a) shows the configuration of the fingers. Finger actuator modules 1 and 2 construct the MCP joint of the finger, and finger actuator modules 3 and 4 construct the PIP and DIP, respectively. All actuator modules are simply serially connected, allowing the joint-level modularization.

It must be noted that the joint alignment of the CMC of the thumb includes a roll joint (CMC-2) as the fingers. Hence, the thumb can be modularized in a similar manner as the fingers. As shown in Fig. 7(a), thumb actuator modules 1 and 2 construct the CMC joint of the thumb, and thumb actuator modules 3 and 4 construct the MP and IP joints, respectively. Similarly to the fingers, all serially connected actuator modules in the thumb allows the joint-level modularization.

The joint alignment of the thumb was devised with the consideration of the thumb opposability. The opposability of the thumb can be evaluated using a well-known clinical test method called the Kapandji test or Kapandji score [17]. The method assesses the capability of the tip of the thumb to touch a specific position of the hand. There are ten different positions from score 1 (radial side of the proximal phalanx of the index finger) to score 10 (distal palmar crease) in order of difficulty. The KITECH-Hand was designed to be able to touch all of the positions in the Kapandji test. Fig. 8 shows two representative examples of the Kapandji test including score 6, tip of the little finger, and score 10, distal

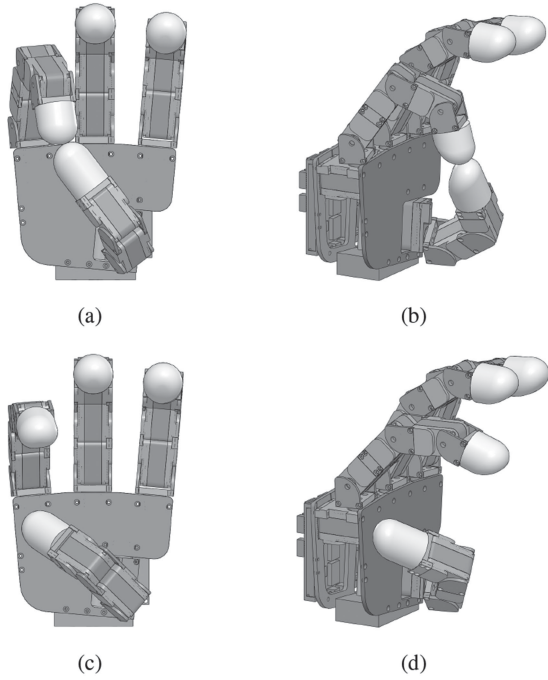


Fig. 8. Kapandji score tests (the ring finger is considered as a little finger for the purpose of test). (a) and (b) Kapandji score 6 (touching tip of the ring finger). (c) and (d) Kapandji score 10 (touching the distal palmar crease).

palmar crease (the little-finger test was replaced with the ring finger due to the absence of the little finger in the KITECH-Hand). As shown in the figure, the proposed thumb structure was able to achieve the highest score of the Kapandji test.

B. Electronics

The KITECH-Hand is designed to be equipped with embedded electronics for driving and low-level control of the hand. In combination, these are referred to as the subcontroller. As a result, DC power and digital communication cables are required only for the external connection. Fig. 9 shows a block diagram describing the electronic components of the robotic hand and communication flows between the embedded and external components. The subcontroller conducts the internal current servoing loop in response to a desired joint torque command from the external main controller and feeds the actual joint position back to the main controller. This subsection addresses the subcontroller. The main controller is not a primary topic of this paper, but will be briefly explained in Section IV-B.

The subcontroller consists of a hand communication unit (HCU), an array of actuator control units (ACUs), and PSUs. Fig. 10 shows the physically implemented electronic components. The PSU shown in Fig. 10(a) is embedded in the actuator module and replaces the original electronic parts of the commercial servo module. The PSU measures the absolute angular position of the actuator module using an analog potentiometer and an analog-to-digital converter. The digitized absolute positions of the joints are read by the HCU shown in Fig. 10(b) via a daisy-chained serial peripheral interface at

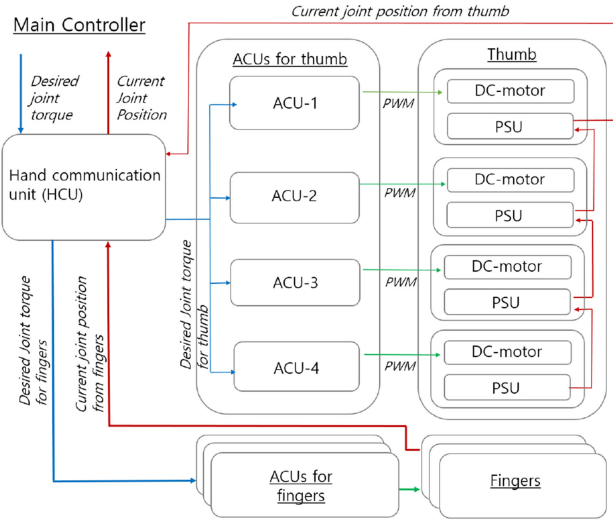


Fig. 9. Schematic diagram of the subcontroller of the KITECH-Hand and data flow in the control system. The blue and red arrows are the desired joint torque and joint position feedback, respectively. Green arrows mean pulse width modulation (PWM) input to actuator modules. In this schematic, the internal structure of the subcontroller for the thumb is depicted in detail; the other fingers are abbreviated in the bottom of the figure.

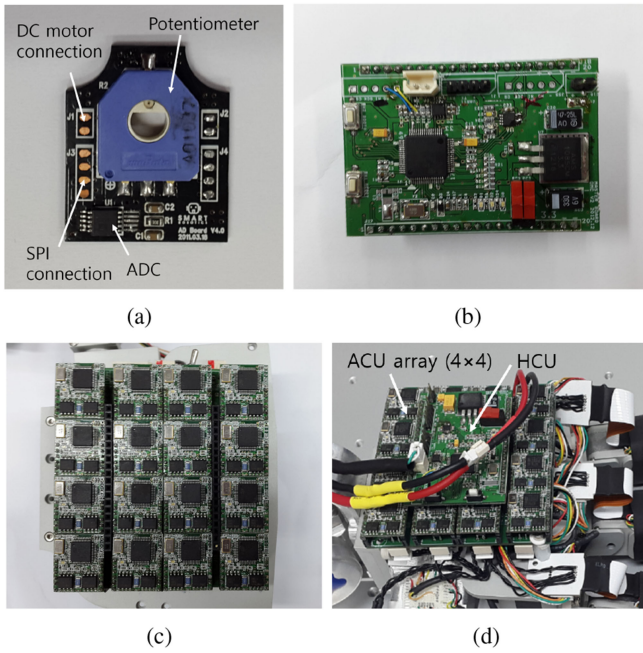


Fig. 10. Subcontroller electronics. (a) PSU. (b) HCU. (c) ACU array. (d) Palm of the KITECH-Hand with installed electronics.

a frequency of 333 Hz. The HCU communicates with the external main controller via a control area network (CAN) channel, updating the position data and receiving new joint torque commands. The command torque is passed to the ACU array shown in Fig. 10(c). The ACU includes a current measurement circuit and a microcontroller unit (MCU, STM32F103C8, ST Microelectronics) and implements joint torque control based on current servoing, which uses a conventional PID control scheme.

TABLE V
MECHANICAL AND ELECTRONIC SPECIFICATIONS OF THE KITECH-HAND

Quantity	Value
Number of fingers	three fingers and a thumb
Degree of freedom	16 DOF
Dimension	35.8 mm × 19.5 mm × 25 mm
Total weight	0.9 kg
Max. Payload	1.5 kg at envelop grasping
Rated Power	5 A at standby, 8 A at grasping, @ 8 V
Communication	CAN

Considering the mechanical friction at the speed reducer, the joint torque at the output shaft τ can be estimated as follows:

$$\tau = k_m i - \tau_f \quad (3)$$

where i and k_m denote the measured current and the motor coefficient, respectively. τ_f is the friction torque, which is a nonlinear function of joint speed. Since it is hard to define τ_f , (3) is simplified in this research as follows:

$$\tau = k_i i \quad (4)$$

where i denotes the measured current and k_i represents the system identification constant, which is experimentally determined. The feasibility and the range of application of this estimation are experimentally investigated in Section IV-A.

The HCU and the ACU array are installed on the palm of the hand, as shown in Fig. 10(d). The total size of the electronic parts installed on the palm is 75 mm × 80 mm × 24 mm.

Table V lists the mechanical and electric specifications of the KITECH-Hand. As mentioned Section I, the weight of the KITECH-Hand, including all electronics, was 0.9 kg. In the table, the payload means the maximum weight that the KITECH-Hand is able to hold with power-grasping mode. The payload value was obtained in an experiment grasping a bottle filled with water.

IV. EXPERIMENTS

The main objectives of this section are to experimentally evaluate the manipulation capability of the KITECH-H, and to determine whether the KITECH-Hand can mimic the human grasping motion effectively despite the modified MCP joint configuration of the fingers. Before addressing the main objectives, the performance of the subcontroller, which is a prerequisite for carrying out the main objectives, is evaluated in advance.

A. Torque Control

As discussed in Section III-B, the KITECH-Hand is controlled using a joint torque control approach based on current servoing. In this subsection, the performance of the current controller is investigated first, and then, the applicability and the possible range of application of contact force estimation according to (4) are determined.

The current controller was implemented in the ACU shown in Fig. 10(c) using a conventional PID control manner. The top of Fig. 11(a) shows the controller's response with respect

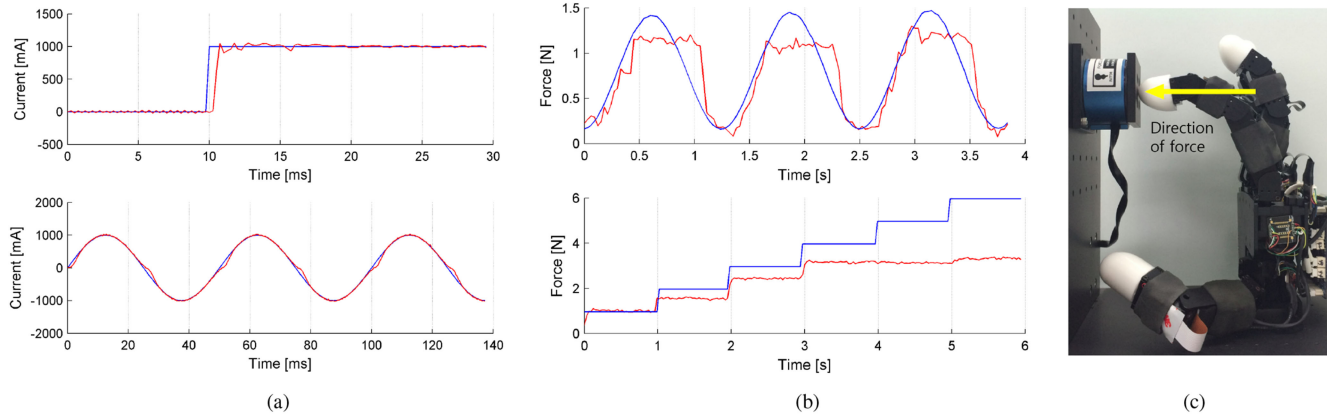


Fig. 11. Current controller and contact force control performance using it. (a) Current response to a step and a sinusoidal input. The desired and measured values are shown in blue and red, respectively. (b) Contact force response to the sinusoidal and incremental input. (c) Contact force experimental setup.

to a step input of 1000 mA, which is the rated current of the actuator module. The settling time was measured to be 2.6 ms. After the period of settling, the steady-state error calculated by the normalized root-mean-square error (NRMSE), i.e., the root-mean-square error divided by the maximum input, was 0.014. The bottom of Fig. 11(a) shows the current response to a sinusoidal input with an amplitude and a period of 1000 mA and 50 ms, respectively. The response generally matches the input curve well. The calculated NRMSE for the experiment was 0.019.

Based on the current controller, the contact force control performance was investigated. Fig. 11(c) shows the experimental setup for the experiment. The robot hand was fixed on a stable ground surface, and a six-axis reference force sensor (IFS-53M31A25, JR3, Japan) was fixed on a vertical plate that was tightly fixed to the ground. The desired contact force was converted to the joint current command using (4), and the actual contact force was recorded at the reference sensor. The top of Fig. 11(b) shows the force response to a sinusoidal contact force input in the X -direction (minus Z -direction at the reference sensor) with an amplitude and a period of 1 N and 1 s, respectively. The response generally matched the input force, with an acceptable degree of error. The error can have various causes, such as inaccurate modeling of the system identification constant, k_i , positioning error in the experimental setup, and measurement error at the reference sensor itself. The calculated NRMSE for the experiment was 0.168.

To investigate the force range over which the contact force control scheme is applicable, a continuously increasing step input experiment was conducted. The experimental result plotted in the bottom of Fig. 11(b) shows that the output force increased nonlinearly from 1 to 4 N input with steady-state errors, and after that, the output force hardly increased, because of saturation of the output force of the actuator modules. From the experimental results, it can be seen that the acceptable contact force range for a finger is 0–4 N, with a maximum NRMSE of 0.226 at 4 N (0.904 N in RMSE).

The force control experiments showed the applicability of contact force control without force sensors. The permissible er-

ror may be different depending on the type of task. If more precise control is required, nonlinear modeling can be utilized instead of (4) to reduce the steady-state errors shown in Fig. 11(b). In this research, the contact force range was set to 0–4 N, accepting the residual errors.

B. In-Hand Manipulation

In this subsection, the manipulation capability of the KITECH-Hand is experimentally demonstrated through in-hand object manipulation tests. The aim of the experiment is to verify the in-hand manipulation ability of the KITECH-hand, which was anticipated in Section II-C. Before addressing the test results, the main controller mentioned in Section III-B is briefly introduced. A grasping method called “advanced blind grasping,” which was a previous field of study of the present authors aimed at grasping and manipulating objects of unknown shape [18], was applied. The method finds the desired contact force vectors at the fingertips that satisfy force equilibrium around a point called the geometric centroid, which can be obtained from the position of the contact spots whose values are known. Once the robotic hand grasps an object, the in-hand manipulation of the object can be realized by simply relocating the geometric centroid to the desired position and orientation and recalculating the desired contact force. With the desired contact force, a control input based on “passivity-based control,” also known as the “virtual spring-damper hypothesis,” is applied as follows [19], [20]:

$$\tau_i = -D_i \dot{q}_i + J_i^T f_i + \tau_g, \quad i = 1, 2, 3, \dots \quad (5)$$

where τ_i is the desired joint torque vector of the i th finger, D_i is a damping coefficient matrix obtained from the inertia matrix of the finger [21], \dot{q}_i is an angular velocity vector of the joints, and J_i^T is a Jacobian transposed matrix of the i th finger. f_i and τ_g are the desired contact force vector at the fingertip and the gravity compensation torque vector, respectively. The damping gain D_i prevents the null-space motion of the finger. In this controller, there is no force feedback loop, and the fingertip contact force and f_i are controlled in a feedforward manner.

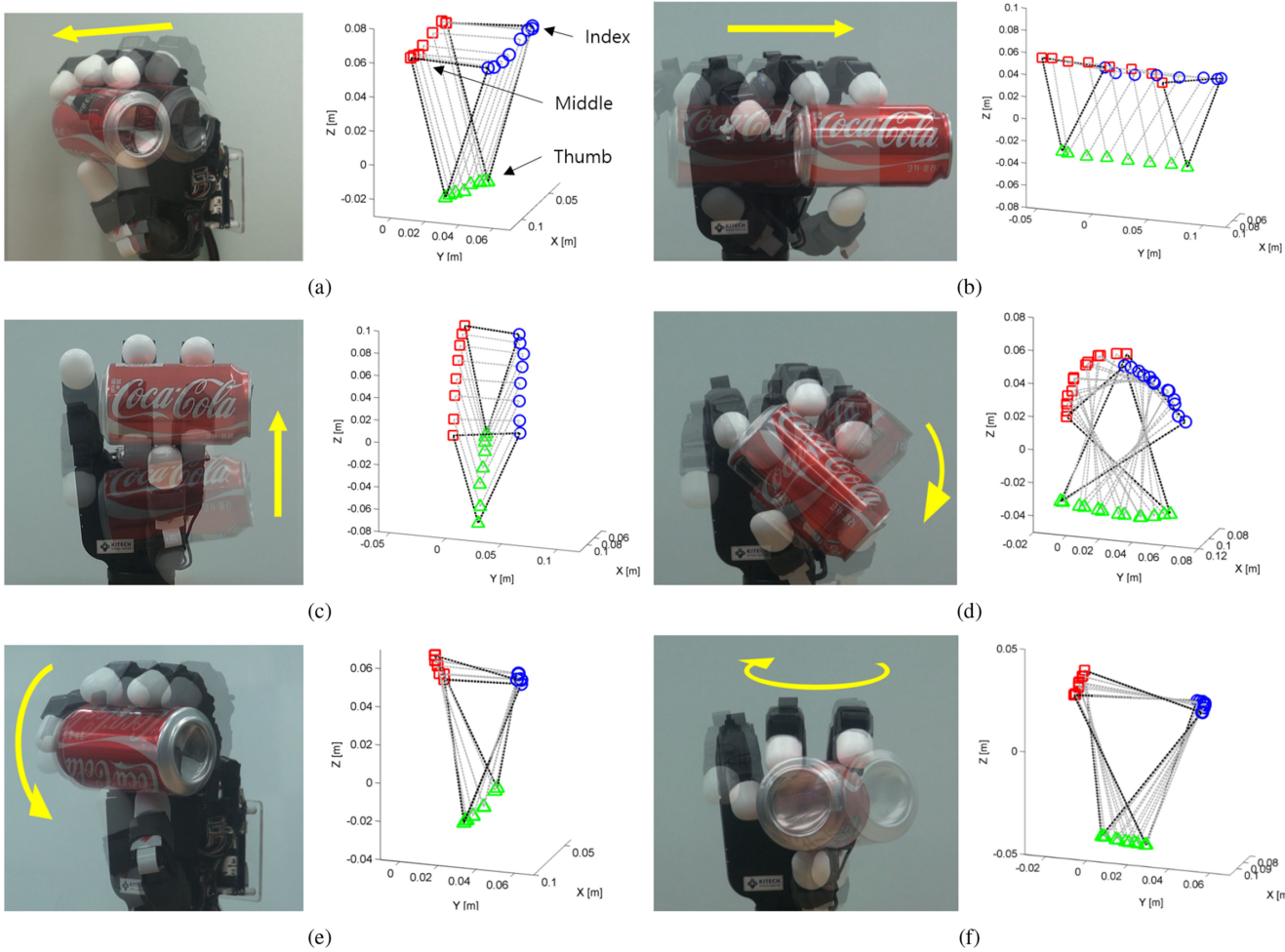


Fig. 12. Object in-hand manipulation along each axis. (a)–(c) Object translation along X -, Y -, and Z -axis, respectively. (d)–(f) Object rotation along X -, Y -, and Z -axis.

This feature enables the robot to perform contact force control with low-cost electronics with a relatively low control frequency and without requiring costly F/T sensors.

In this research, the dexterity of the KITECH-Hand was experimentally shown by translating and rotating the geometric centroid of the grasped object using the control strategy mentioned above. The experiments involved pinch-grasping a cylindrical object (empty Coca Cola can) whose diameter is 60 mm with two fingers and the thumb. In the experiments, weight of the object was neglected.

Fig. 12(a) shows the in-hand translation sequence of the object along the X -axis. As shown in the figure, the human-like shape of the fingertips helps the natural rolling motion of the object for the translation. The trajectory of the triangle built by three contact points during the experiment is presented in the right figure of Fig. 12(a). During the experiment, the object was translated in task space over a distance of 4.5 cm along the X -axis. The object in-hand translation sequence along the Y -axis is shown in Fig. 12(b). The right figure of Fig. 12(b) shows the contact triangles during the translation. This demonstration is a representative example to show the dexterity of the KITECH-Hand. In fact, the object translation along the Y -axis is hardly possi-

ble for conventional anthropomorphic robotic hands or human hands, since the translation motion is transverse of the singular position of the MCP joints. In the case of the KITECH-Hand, the object translation with a displacement of 12.5 cm along the Y -axis was possible. Meanwhile, the object in-hand translation result along the Z -axis is shown in Fig. 12(c) with the contact triangle trajectory. The displacement during the experiment was 10 cm.

Subsequent to the translation tests, object in-hand rotation experiments were carried out. Fig. 12(d) shows the in-hand rotation sequence and the contact triangle trajectory along the X -axis. During the experiment, the object was translated 60° along the axis. The experiment sequence shows that the object was rotated smoothly with rolling contact. This is similar to a human's in-hand rolling despite the different kinematic structure of the MCP joints of the fingers. The results of in-hand rotation along the Y -axis are shown in Fig. 12(e). As shown in the right figure of Fig. 12(e), the final contact triangle was rotated over an angle of 55° from its starting position. Finally, the results of object in-hand rotation along the Z -axis are shown in Fig. 12(f). The rotational displacement during the experiment was 28°, as shown in the right figure of Fig. 12(f).

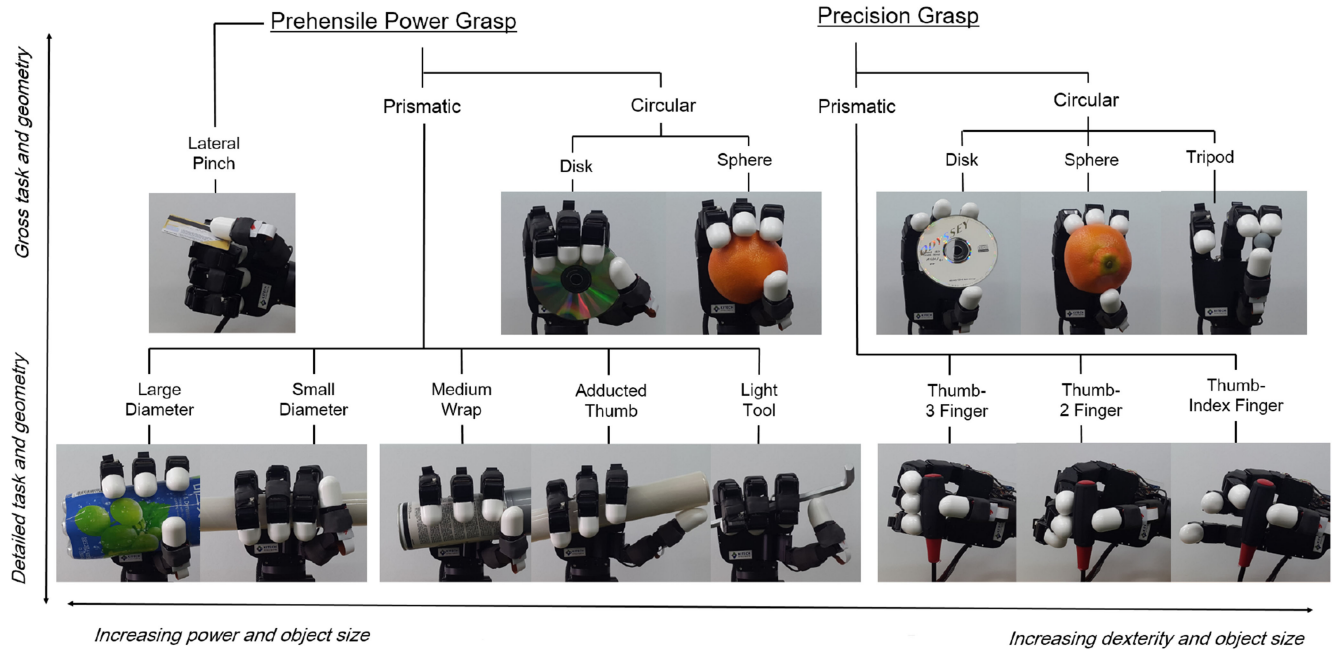


Fig. 13. Grasping poses performed by the KITECH-Hand according to the Cutkosky taxonomy. The grasping pose with the thumb and the four fingers was not included due to the absence of the little finger.

The object in-hand manipulation experiments presented in this subsection effectively visualize the remarkable dexterity of the KITECH-Hand, even occasionally surpassing the capabilities of the human hand. The experimental results show that the distinct MCP joint structure not only simplifies the mechanical complexity, but also increases the dexterity of the anthropomorphic robotic hand. Through the experiments, it is expected that the enhanced dexterity can be applied to various tasks in factory automation.

C. Cutkosky Taxonomy Test

The goal of this subsection is to determine whether the KITECH-Hand can mimic the human grasping motion effectively despite the modified configuration of the MCP joint in its fingers. It is explicit that a very small number of poses cannot be performed by the KITECH-Hand due to the absence of abduction and adduction, e.g., lateral pinching in a scissors-like motion using the index and the middle fingers. However, it should be noted that the main applications of robotic hands are in factory automation and service robotics; therefore, their performance should be evaluated in that context.

The Cutkosky taxonomy is a widely accepted classification method for the grasping motion of the human hand required for common machining tasks [22]. The taxonomy proposes 16 different types of grasp poses, which are largely classified into power grasping and precision grasping. By using the KITECH-Hand, a static evaluation was conducted to determine if the hand can perform the grasp poses proposed in the Cutkosky taxonomy.

Fig. 13 shows the results of the evaluation. The KITECH-Hand was able to perform all of the poses (eight power-grasping and six precision-grasping poses) successfully. Five-

finger pinch grasping using the thumb and four fingers could not be included due to the absence of the little finger.

The results of this test show that the rolling motion in the MCP joint in the fingers is able to effectively cover the role of abduction and adduction of the human hands in most grasping poses important to robotic hands. This result is consistent with the observation that the main role of the abduction and adduction of the human hand is to build the intersection volume of the workspace, which can be alternatively performed by adding the rolling motion in the MCP joints.

V. CONCLUSION

In this research, an anthropomorphic robotic hand, KITECH-Hand, was presented. The key difference of the KITECH-Hand is its “roll–pitch”-type MCP joint in the fingers, which provides kinematic and mechanical advantages. Through kinematic analysis, it was shown that the proposed structure remarkably increases the thumb opposability and fingertip manipulability in the common workspace between the thumb and fingers compared to conventional “yaw–pitch”-type robotic hands. These features are particularly helpful for object in-hand manipulation using the robotic hands without palm motion.

From a mechanical perspective, the robotic hand was designed with a joint-level modularization concept, namely, the robotic hand consists of mechanically identical and fully functional joint modules. This approach makes the robot hand mechanically simpler and lowers its production and maintenance costs.

The object manipulation capability of the KITECH-Hand was experimentally demonstrated via intensive in-hand manipulation and various object grasping tests. The in-hand manipulation results showed that the dexterous manipulation

capability of the KITECH-Hand exceeded even the human hand capability. Through the Cutkosky tests, it was shown that the KITECH-Hand is able to perform most of the grasping poses that are important to perform complex human tasks.

The KITECH-Hand is now commercialized, under the “Allegro Hand” [23] name, and is one of the lowest cost anthropomorphic robotic hands commercially available at present, with fully actuated 16-DOF joints. Its high dexterity, fast response, and stable grasping capability have contributed to cutting-edge research on robotic manipulation [24]–[27].

ACKNOWLEDGMENT

The authors would like to thank Hyeyonjun Park with the Korea Institute of Industrial Technology for his efforts in experiments conducted for this research.

REFERENCES

- [1] J. Butterfaß, M. Grebenstein, H. Liu, and G. Hirzinger, “DLR-hand II: Next generation of a dexterous robot hand,” in *Proc. IEEE Int. Conf. Robot. Autom.*, 2001, pp. 109–114.
- [2] H. Kawasaki, T. Komatsu, and K. Uchiyama, “Dexterous anthropomorphic robot hand with distributed tactile sensor: Gifu hand II,” *IEEE/ASME Trans. Mechatronics*, vol. 7, no. 3, pp. 296–303, Sep. 2002.
- [3] T. Mourit, H. Kawasaki, K. Yoshikawa, J. Takai, and S. Ito, “Anthropomorphic robot hand: Gifu hand III,” in *Proc. Int. Conf. Control, Autom. Syst.*, Oct. 2002, pp. 1288–1293.
- [4] D. Choi, S. Shin, J. C. Koo, H. R. Choi, and H. Moon, “The SKKU hand: Work in progress,” in *Proc. IEEE Int. Conf. Ubiquitous Robot. Ambient Intell.*, Nov. 2012, pp. 437–438.
- [5] S. Ryew and H. Choi, “Double active universal joint (DAUJ): Robotic joint mechanism for human-like motions,” *IEEE Trans. Robot. Autom.*, vol. 17, no. 3, pp. 290–300, Jun. 2001.
- [6] A. D. Deshpande *et al.*, “Mechanisms of the anatomically correct testbed hand,” *IEEE/ASME Trans. Mechatronics*, vol. 18, no. 1, pp. 238–250, Feb. 2013.
- [7] J. Martin and M. Grossard, “Design of a fully modular and backdrivable dexterous hand,” *Int. J. Robot. Res.*, vol. 33, no. 5, pp. 783–798, 2014.
- [8] M. Grossard, J. Martin, and G. F. d. C. Pacheco, “Control-oriented design and robust decentralized control of the CEA dexterous robot hand,” *IEEE/ASME Trans. Mechatronics*, vol. 20, no. 4, pp. 1809–1821, Aug. 2015.
- [9] F. Lotti, P. Tiezzi, G. Vassura, L. Biagiotti, G. Palli, and C. Melchiorri, “Development of UB hand 3: Early results,” in *Proc. IEEE Int. Conf. Robot. Autom.*, 2005, pp. 4488–4493.
- [10] C. Melchiorri, G. Palli, G. Berselli, and G. Vassura, “Development of the UB hand IV: Overview of design solutions and enabling technologies,” *IEEE Robot. Autom. Mag.*, vol. 20, no. 3, pp. 72–81, Sep. 2013.
- [11] L. B. Bridgwater *et al.*, “The Robonaut 2 hand-designed to do work with tools,” in *Proc. IEEE Int. Conf. Robot. Autom.*, May 2012, pp. 3425–3430.
- [12] J.-H. Bae, S.-W. Park, J.-H. Park, M.-H. Baeg, D. Kim, and S.-R. Oh, “Development of a low cost anthropomorphic robot hand with high capability,” in *Proc. IEEE/RSJ Int. Conf. Intell. Robot. Syst.*, Oct. 2012, pp. 4776–4782.
- [13] H. Wang, S. Fan, and H. Liu, “An anthropomorphic design guideline for the thumb of the dexterous hand,” in *Proc. IEEE Int. Conf. Mechatronics Autom.*, Aug. 2012, pp. 777–782.
- [14] J. Rastegar and B. Fardaneh, “Manipulation workspace analysis using the Monte Carlo method,” *Mech. Mach. Theory*, vol. 25, no. 2, pp. 233–239, 1990.
- [15] J. Angeles and F. C. Park, “Performance evaluation and design criteria,” in *Springer Handbook of Robotics*. New York, NY, USA: Springer, 2008, pp. 229–244.
- [16] T. Yoshikawa, “Manipulability of robotic mechanisms,” *Int. J. Robot. Res.*, vol. 4, no. 2, pp. 3–9, 1985.
- [17] A. Kapandji, “Clinical test of apposition and counter-apposition of the thumb,” *Ann. Chirurgie Main: Organe Officiel des Soc. Chirurgie Main*, vol. 5, no. 1, pp. 67–73, 1985.
- [18] J.-H. Bae, S.-W. Park, D. Kim, M.-H. Baeg, and S.-R. Oh, “A grasp strategy with the geometric centroid of a groped object shape derived from contact spots,” in *Proc. IEEE Int. Conf. Robot. Autom.*, May 2012, pp. 3798–3804.
- [19] S. Arimoto, *Control Theory of Nonlinear Mechanical Systems*. Oxford, U.K.: Oxford Univ. Press, 1996.
- [20] S. Arimoto, M. Sekimoto, H. Hashiguchi, and R. Ozawa, “Natural resolution of ill-posedness of inverse kinematics for redundant robots: a challenge to Bernstein’s degrees-of-freedom problem,” *Adv. Robot.*, vol. 19, no. 4, pp. 401–434, 2005.
- [21] S. Arimoto, *Control Theory of Multi-fingered Hands: A Modelling and Analytical Mechanics Approach for Dexterity and Intelligence*. New York, NY, USA: Springer, 2008.
- [22] M. R. Cutkosky, “On grasp choice, grasp models, and the design of hands for manufacturing tasks,” *IEEE Trans. Robot. Autom.*, vol. 5, no. 3, pp. 269–279, Jun. 1989.
- [23] [Online]. Available: <http://www.simlab.co.kr/Allegro-Hand.htm>
- [24] S. Kim, A. Shukla, and A. Billard, “Catching objects in flight,” *IEEE Trans. Robot.*, vol. 30, no. 5, pp. 1049–1065, Oct. 2014.
- [25] M. Li, H. Yin, K. Tahara, and A. Billard, “Learning object-level impedance control for robust grasping and dexterous manipulation,” in *Proc. IEEE Int. Conf. Robot. Autom.*, May 2014, pp. 6784–6791.
- [26] J. Jo, S.-K. Kim, Y. Oh, and S.-R. Oh, “Strategy of internal force design without object com information,” in *Proc. IEEE Int. Conf. Ubiquitous Robot. Ambient Intell.*, Oct. 2013, pp. 167–170.
- [27] D.-H. Lee, U. Kim, H. Jung, and H. R. Choi, “A capacitive-type novel six-axis force/torque sensor for robotic applications,” *IEEE Sens. J.*, vol. 16, no. 8, pp. 2290–2299, Apr. 2016.



Dong-Hyuk Lee received the B.S. degree in mechanical engineering, the M.S. degree in mechatronics engineering, and the Ph.D. degree in mechanical engineering from Sungkyunkwan University, Suwon, South Korea, in 2008, 2010, and 2015, respectively.

Since 2015, he has been with the Robot Cognition and Control Laboratory, Korea Institute of Industrial Technology, Ansan, South Korea, where he is a Postdoctoral Researcher. His research interests include force/tactile sensors for robotics applications and dexterous manipulation for industrial robotics.



Jae-Han Park (M’10) received the B.S. degree in electrical engineering from Donga University, Busan, South Korea, in 1998, and the M.S. degree in electronic engineering from Busan University, Busan, in 2000. Since 2010, he has been working toward the Ph.D. degree in electronic engineering at Korea University, Seoul, South Korea.

He is a Senior Research Scientist with the Robot Cognition and Control Laboratory, Robot R&D Group, Korea Institute of Industrial Technology, Ansan, South Korea. His research interests include 3-D data processing and cognition-based robotics.



Sung-Woo Park received the B.S. degree in mechanical engineering from Donga University, Busan, South Korea, in 2005, and the M.S. degree in intelligent robotics from the Korea University of Science and Technology, Daejeon, South Korea, in 2012.

He was a Staff Engineer at LG Electronics, Seoul, South Korea, from 2005 to 2007. He is a CTO with MECHA TNS. His current research interests include factory automation, robot manipulation, robot hand, and embedded systems.



3-D space.

Moon-Hong Baeg received the B.S. and M.S. degrees in control and measurement engineering from Seoul National University, Seoul, South Korea, in 1982 and 1984, respectively, and the Ph.D. degree in electrical engineering from Tokyo University, Tokyo, Japan, in 1995.

He is a Principal Research Scientist with the Robot Cognition and Control Laboratory, Robot R&D Group, Korea Institute of Industrial Technology, Ansan, South Korea. His research interests include robot vision and robot cognition in



Ji-Hun Bae (M'04) received the B.S. and M.S. degrees in electrical engineering from Myongji University, Seoul, South Korea, in 1999 and 2001, respectively, and the Ph.D. degree in robotics from Ritsumeikan University, Kyoto, Japan, in 2004.

He is a Principal Research Scientist with the Robot Cognition and Control Laboratory, Robot R&D Group, Korea Institute of Industrial Technology, Ansan, South Korea. From 2004 to 2006, he was a Postdoctoral Fellow at the 21st Century COE Program, Ritsumeikan University. He was a Senior Researcher at Korea Institute of Robot Convergence, Pohang, South Korea, from 2006 to 2008, and a Postdoctoral Fellow at the Korea Institute of Science and Technology from 2008 to 2009. His research interests include control algorithms for robotic hands and arms, coordinated hand-arm control, two-handed manipulation, and biological control.